Protonation-dependent stepped rotation of the F-type ATP synthase c-ring observed by single-molecule measurements

Received for publication, May 31, 2017, and in revised form, August 2, 2017 Published, Papers in Press, August 25, 2017, DOI 10.1074/jbc.M117.799940

Seiga Yanagisawa and Wayne D. Frasch[1]

From the School of Life Sciences, Arizona State University, Tempe, Arizona, 85287-4501

Edited by Wolfgang Peti

The two opposed rotary molecular motors of the F_0F_1-ATP synthase work together to provide the majority of ATP in biological organisms. Rotation occurs in 120° power strokes separated by dwells when F_1 synthesizes or hydrolyzes ATP. F_0 and F_1 complexes connect via a central rotor stalk and a peripheral stator stalk. A major unresolved question is the mechanism in which the interaction between subunit-a and rotating subunit-c–ring in the F_0 motor uses the flux of H^+ across the membrane to induce clockwise rotation against the force of counterclockwise rotation driven by the F_1-ATPase. In single-molecule measurements of F_0F_1 embedded in lipid bilayer nanodiscs, we observed that the ability of the F_0 motor to form transient dwells increases with decreasing pH. Transient dwells can halt counterclockwise rotation powered by the F_1-ATPase in steps equivalent to the rotation of single c-subunits in the c-ring of F_0, and can push the common axle shared by the two motors clockwise by as much as one c-subunit. Because the F_0 proton half-channels that access the periplasm and the cytoplasm are exposed to the same pH, these data are consistent with the conclusion that the periplasmic half-channel is more easily protonated in a manner that halts ATPase-driven rotation by blocking ATPase-dependent proton pumping. The fit of transient dwell occurrence to the sum of three Gaussian curves suggests that the asymmetry of the three ATPase-dependent 120° power strokes imposed by the relative positions of the central and peripheral stalks affects c-subunit stepping efficiency.

The F-ATP synthases, located in eubacteria, mitochondria, and chloroplasts, are members of a family of rotary molecular motors that also include archaeal A-ATP synthases, bacterial A/V-like ATP synthases, and eukaryotic vacuolar V-ATPases (1). The F-ATP synthases are composed of two opposed rotary motors known as the membrane-embedded F_0, and the extrinsic membrane protein complex F_1 (Fig. 1). These motors are connected by a central stalk that serves as the rotor and a peripheral stalk that is a component of the stator (2). In *Escherichia coli*, as in most organisms, the largest single source of cellular ATP is that made by the F_0F_1-ATP synthase.

This project was supported by National Institutes of Health Grant R01 GM097510 (to W. D. F.). The authors declare that they have no conflicts of interest with the contents of this article. The content is solely the responsibility of the authors and does not necessarily represent the official views of the National Institutes of Health.

[1] To whom correspondence should be addressed. Tel.: 480-965-8663; E-mail: frasch@asu.edu.

Synthesis of ATP from ADP and inorganic phosphate (P_i) is catalyzed by F_1 in response to a transmembrane electrochemical gradient used by F_0 to force the rotor in the clockwise (CW)[2] direction as viewed from the periplasm of *E. coli* (3). In so doing, *E. coli* F_0, which is specific for protons, consumes the gradient by transporting protons across the membrane. The F_1 motor can hydrolyze ATP to drive the rotor counterclockwise (CCW) and pump protons (4, 5). However, under steady state conditions, the F_0F_1-ATP synthase maintains the [ATP]/[ADP] [P_i] ratio far from equilibrium (6–8).

The three catalytic sites for ATP synthesis/hydrolysis are located at the interfaces of α- and β-subunit heterodimers that comprise the $(\alpha\beta)_3$-ring of the F_1-ATPase, which serves as the stator (9). The rotor consists of the γ-subunit that protrudes from the center of the $(\alpha\beta)_3$-ring, the ϵ-subunit, and the ring of c-subunits of F_0. During ATPase-driven rotation, each 120° power stroke occurs as the result of the binding of an ATP to the empty catalytic site, whereas product release occurs at an adjacent site (10). Hydrolysis of ATP occurs at the third site during catalytic dwells that separate the power strokes. Three states of the *E. coli* F_0F_1 structure were revealed by single-particle cryo-EM in which the axle subunits γ and ϵ were rotated in 120° increments from the peripheral stalk that is a component of the stator (11).

In the F_0 motor, proton translocation-dependent rotation of the c-ring results from events in which half-channels in stator subunit-a protonate and deprotonate cAsp^{61} on each c-subunit. Subunit-a of *E. coli* F_0F_1 folds in a manner similar to that observed in F_0 structures from other organisms for which the structure is known (11–14). Subunit-a helices 1–4 anchor the b-subunits of the peripheral stalk, and are distal from the c-ring. Helices 3–6 are oriented at an oblique angle to the membrane plane where C-terminal helices (5 and 6) are proximal to the c-ring. The connection between the distal and proximal helices contains two 3_{10}-helical segments (Fig. 1, *B* and *C*, *helices I and II*) that vary in conformation among known structures.

Subunit-a residues aAsn^{214}, aGlu^{219}, aHis^{245}, and aGln^{252} on helices 5 and 6 have been implicated in proton translocation as part of the periplasmic half-channel that serves as the import channel during proton gradient–powered c-ring rotation (CW) for ATP synthesis (15–17). To date, the only residue known to participate in the cytoplasmic half-channel, which serves as the import channel for ATPase-driven proton pumping, is aGlu^{196} (17, 18). The two half-channels are separated by aArg^{210} that

[2] The abbreviations used are: CW, clockwise; CCW, counterclockwise; n-F_0F_1, nanodisc-embedded F_0F_1 ATP synthase.

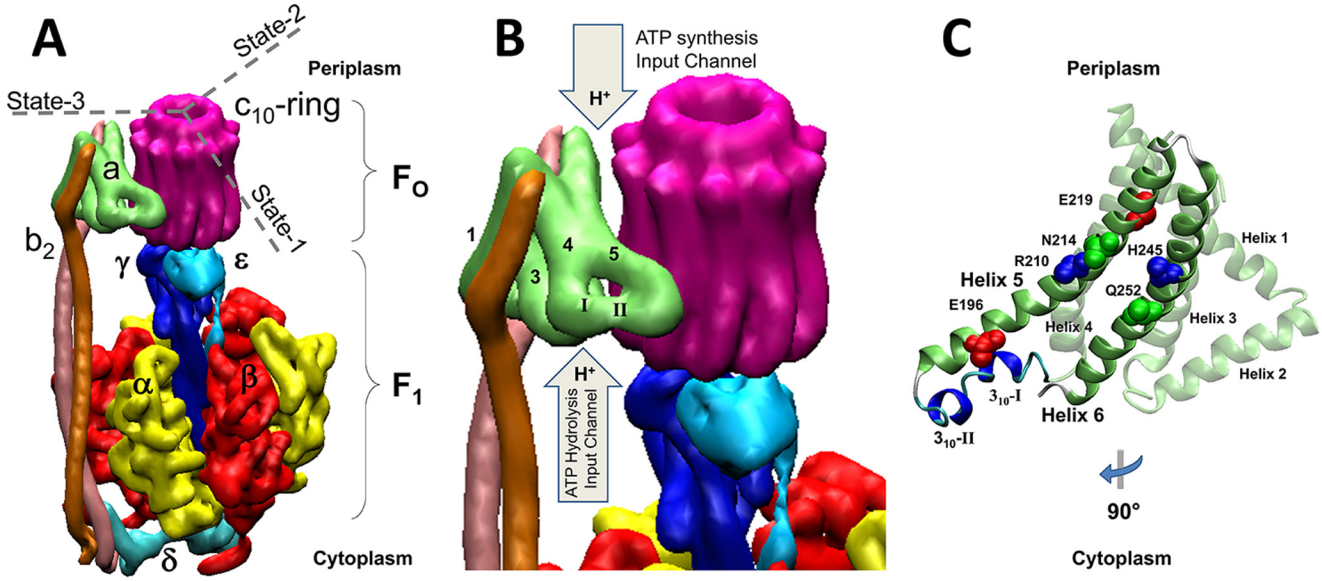

Figure 1. Structural features of the F_0F_1-ATP synthase are shown. *A*, subunit organization of the *E. coli* F_0F_1 ATP synthase (11) (PDB reference ID 5T4O). *B*, organization of helices in subunit-a and approximate locations of proton translocation half-channels with access for protons from the periplasm and cytoplasm of *E. coli* that serve as the input channels during ATP synthesis and hydrolysis, respectively. Two 3_{10}-helical segments (I and II) in the subunit-a segment that connect helices 4 and 5. *C*, structure of subunit-a rotated 90° clockwise from *A* and *B* that shows the position of residues implicated in proton translocation, and 3_{10}-helical segments 1 and 2.

effectively deprotonates cAsp[61] as each successive c-subunit rotates into close proximity of its resonance-stabilized positive charge (19).

Rates of ATP synthesis catalyzed by the F-ATP synthase can approach 400–600 ATP s^{-1} (20–22). This equates to 500–750 μs per proton translocated during the rotational stepping of single c-subunits in *E. coli* that has a c_{10}-ring. The ability to observe single c-subunit stepping of the c-ring on this time scale was first achieved in single-molecule experiments by monitoring ATPase-driven rotation using a gold nanorod attached to the c-ring of F_0F_1 embedded in lipid bilayer nanodiscs (n-F_0F_1) (23). Although some power strokes rotated CCW in continuous 120° events, many were periodically interrupted by "transient dwells." These dwells occurred at an average interval of ~36°, consistent with single c-subunit stepping of the c_{10}-ring of *E. coli* F_0F_1. The duration of transient dwells ranged from 50 to175 μs. Although somewhat shorter than the duration of c-subunit stepping anticipated during ATP synthesis, transient dwells are observed in the presence of high ATP concentrations that optimize ATP hydrolysis in lieu of synthesis. The fraction of power strokes that contain transient dwells can be increased to the point at which they are present in all power strokes of most data sets (~80% average occurrence in all power strokes) through the use of viscosity-dependent drag to decrease the angular velocity of the F_1-ATPase power stroke.

Mutations in subunit-a and subunit-c have been identified that affect the ability to form transient dwells (18, 23), indicating that these dwells result when subunit-a forms a "leash" with the c-ring that limits CCW rotation to a maximum of ~36° while engaged. Subunit-a was not only observed to halt CCW rotation of the c-ring in n-F_0F_1 but, in >70% of all transient dwells, was also able to push the rotor CW against ATPase-dependent rotation powered by F_1 (18). The extent of CW rotation in the ATP synthesis direction averaged 11°, but could be as much as ~36°, which is equivalent to rotation of the c-ring by one c-subunit relative to subunit-a.

Using proteoliposomes in which the F_1 complex of F_0F_1 is on the outside, high rates of ATP synthesis require transmembrane proton gradients with a $\Delta pH = 3$. This is typically achieved by equilibrating the pH inside the liposome to 5.5 and then rapidly shifting the outside pH to 8.5 (6, 21). Thus far, single-molecule rotation studies of F_0F_1 embedded in nanodiscs have been examined only at pH 8.0. We now present a single-molecule study of the pH dependence of transient dwell formation by n-F_0F_1. The occurrence of transient dwells increased inversely with pH over the pH range of 5.0 to 7.0. Transient dwells formed at low pH at intervals of ~36° lasted an average of 118–158 μs and were able to push the c-ring CW against the force of ATPase-dependent CCW rotation by as much as one c-subunit. These results show that even though both F_0 half-channels were exposed to the same pH, the periplasmic half-channel that serves as the ATP synthase proton import channel is more easily protonated in a manner that halted ATPase-driven rotation by blocking ATPase-dependent proton pumping.

Results

Rotation of the c-ring of single n-F_0F_1 molecules was monitored as a function of time by changes in the intensity of polarized red light scattered from a 80 × 40-nm gold nanorod attached to the c-ring (Fig. 2). For each molecule examined, multiple 5-s data sets of ATP hydrolysis-powered rotation were acquired in the presence of 1 mM Mg-ATP at a data acquisition rate of 100 kHz. At this saturating substrate concentration, *E. coli* F_1 produces power strokes that rotate 120° CCW on a time scale of ~300 μs, which are separated by catalytic dwells with a duration of a few milliseconds (5, 24). The intensity of polarized red light that is scattered from the long axis of the

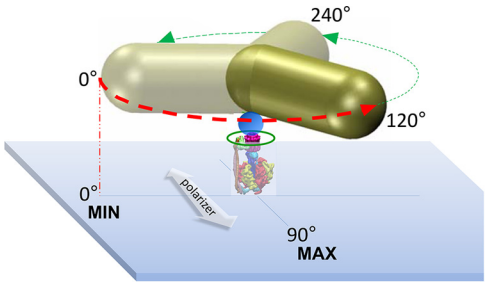

Figure 2. A gold nanorod was used as a probe of rotational position to make single-molecule measurements of F_0F_1 embedded in lipid bilayer nanodiscs (*green circle*). Attachment of F_0F_1 to the microscope slide occurred via His_6 tags on the N termini of the F_1 β-subunits. The c2▽Cys mutation to *E. coli* F_0F_1 (see "Experimental procedures") was biotinylated to attach the gold nanorod (80 × 40 nm) coated with streptavidin (*blue sphere*). The 120° power strokes (*red* and *green dashed arrows*) resulting from F_1-ATPase–dependent CCW rotation in the presence of 1 mM Mg-ATP were monitored by the intensity of polarized red light scattered from the long axis of the nanorod as a function of time. Shorter wavelengths were eliminated by a band-pass filter. Prior to data collection, a polarizing filter (*white arrow*) was aligned for minimum intensity of scattered light at one of the three ATPase-dependent catalytic dwells (0°) such that the intensity during the subsequent power stroke increased and passed through a maximum when the nanorod rotated 90° measured using an avalanche photodiode. These power strokes (*red dashed arrow*) were analyzed for the presence of transient dwells.

nanorod oscillates in a sinusoidal manner as the nanorod rotates relative to the direction of the polarizing filter in the light path of the microscope, which is captured by a single photon detector (25).

Examples of n-F_0F_1 power strokes that contain or lack transient dwells at pH 5.0 are shown in Fig. 3, *A* and *B*, respectively. Prior to data collection of each molecule, the polarizing filter was rotated to minimize the scattered light intensity from one of the three catalytic dwells. During the subsequent power stroke, the light intensity increased through a maximum as the nanorod rotated CCW 90°. Each data set acquired contained ~300 power strokes that fit to these criteria, and were analyzed for the presence of transient dwells. In the absence of transient dwells, the power stroke rotated CCW continuously at angular velocities that were comparable with that of purified F_1-ATPase (26).

Transient dwells that stopped the CCW rotation driven by the F_1-ATPase, and those that rotated the c-ring CW against the force of the F_1 power stroke at pH 5.0, are indicated as *green* and *red* data, respectively (Fig. 3*A*). The average periodicity of transient dwells as a function of pH is shown in Fig. 4*A*. At pH 5.0, transient dwells occurred an average of every 35.3 ± 0.3 (S.E.). This periodicity did not change significantly between pH 5.0 and 9.0, and is consistent with a mechanism in which transient dwells result from stepping by single c-subunits in the c_{10}-ring of *E. coli* F_0F_1.

The duration of transient dwells was ~118 μs at pH 5.0 and at pH 9.0, but increased with pH to a maximum value of ~158 μs at pH 8.0 (Fig. 4*B*), which amounted to a change of ~25% over the pH range examined. In the absence of transient dwells, power strokes rotated the first 90° from the catalytic dwell at pH 5.0 in ~250 μs, which was comparable with power strokes of soluble *E. coli* F_1-ATPase (5, 24). When transient dwells were present, the increase in the time required to rotate 90° resulted from the duration of the transient dwells.

Fig. 5 shows the average percent of transient dwells formed per data set during n-F_0F_1 power strokes as a function of pH, where each data set contained about 300 power strokes. At pH 9.0, about 23% of the power strokes contained transient dwells, and transient dwell formation did not change significantly from this value between pH 9.0 and pH 7.5. However, the occurrence of transient dwells increased with decreasing pH between pH 7.5 and pH 5.0 to an average of ~48% at pH 5.0. The fit of these data to the Henderson-Hasselbach relationship suggested that protonation of a group with a p*K* of 6.3 was necessary to form a transient dwell. However, it is clear that the average changes in transient dwell formation between pH 6.0 and 7.5 did not fit particularly well to the dependence on the protonation of a single group.

The distributions of single-molecule rotation data sets of n-F_0F_1 power strokes at each pH as a function of the percentage of transitions in each data set that contain transient dwells are shown in Fig. 6*A* (*gray bars*). The percentage of transient dwells formed per data set that each contained ~300 power strokes was determined, and the data sets were binned into groups for each 10% occurrence of transient dwells formed. Although the percentage of transient dwells formed per data set shown in Fig. 5 was taken from the averages of these distributions, it is clear that these data did not fit to a normal distribution over the pH range examined. In several data sets at pH values between 5.0 and 6.0, transient dwells formed in 90–100% of the power strokes.

The *E. coli* F_0F_1 structure determined by cryo-EM was observed to exist in three states that differed in the rotary positions of the central stalk relative to the peripheral stalk by 120° (11). To test the hypothesis that the distributions of transient dwells observed in Fig. 6*A* could result in differences of the three structural states, three Gaussian curves for which the probability of forming transient dwells was low (*blue line*), medium (*red line*), and high (*green line*) were generated. The sum of the three Gaussians (*black line*) were fit to the measured distribution at each pH (*gray bars*).

The average values of transient dwells formed represented by each of the three Gaussian curves increased inversely with pH (Fig. 7). The Gaussian fit with the highest probability of forming transient dwells (*green*) increased to the greatest extent, and had an average value of 70% transient dwell formation per data set at pH 5.0.

The distributions of the extent to which subunit-a was able to force the c-ring to rotate CW against the ATPase-driven CCW power stroke during the transient dwell as a function of pH are shown in Fig. 6*B*. The maximal extent of these "backsteps" in the CW direction was about 36°, equivalent to the rotation of the c_{10}-ring by one c-subunit. The distributions of the extent of the backsteps was plotted as a difference from that of pH 5.5 for which the extent of the backstep was lowest (Fig. 6*C*). The average changes in the extent of the backstep as a function of pH were insignificant, ranging from ~11° at pH 5.5 to a maximum of about 13° at pH 7.0. The percentage of transient dwells that contained backsteps varied only by ~13% as a function of pH from a minimum to a maximum of 67 to 80% at pH 5.0 and 7.0, respectively (Fig. 8).

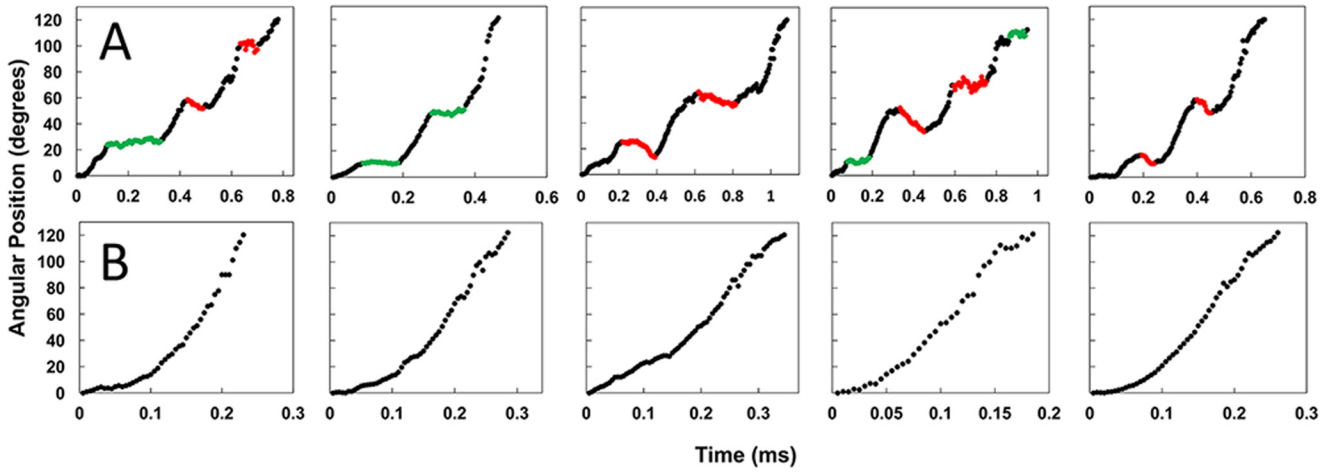

Figure 3. Examples of time-dependent changes in rotational position of n-F_0F_1 during F_1-ATPase–dependent power strokes at pH 5. 0 where transient dwells are present (*A*), or absent (*B*) are shown. Transient dwells where rotation was halted, or contained CW rotation are colored *green* and *red*, respectively.

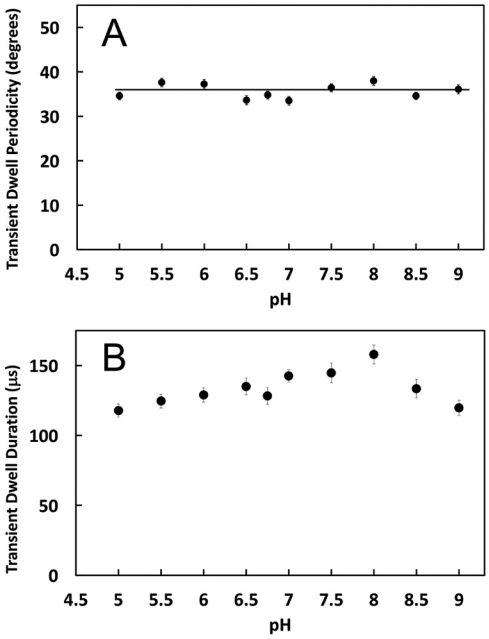

Figure 4. The pH dependence of the average degrees of rotation between transient dwells (*A*), or the duration of transient dwells (*B*) is shown. Vertical bars indicate standard error.

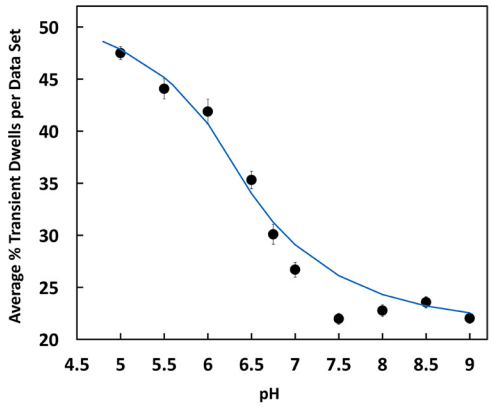

Figure 5. The average percent of transient dwells per data set as a function of pH is shown. Each data set contained ~300 power strokes. The data were fit to a Henderson-Hasselbach dependence for the protonation of a single group with a p*K* of 6.3 (*blue line*). Vertical bars indicate standard error determined from the distributions in Fig. 6*A* (*gray bars*).

Discussion

The results presented here show that the occurrence of transient dwells increases as the pH of the medium becomes more acidic. Subunit-a is the stator component in the F_0 complex that contains both half-channels for proton translocation across the membrane (27). High rates of ATP synthesis are achieved in inverted membrane vesicles of *E. coli* when the periplasmic and cytoplasmic half-channels are exposed to pH 5.5 and 8.5, respectively (6, 21). As a result of this non-equilibrium gradient, protons enter F_0 through the periplasmic half-channel (the ATP synthase input channel) to induce CW rotation of the c-ring. Conversely, ATPase-driven proton pumping occurs as the result of protons entering F_0 from the cytoplasm as the result of CCW rotation induced by ATP hydrolysis in F_1.

Transient dwells result from the ability of subunit-a to interact with subunit-c in a manner that stops ATPase-dependent CCW rotation of the c-ring, and results in CW rotation in the ATP synthesis direction ~ 80% of the time (Fig. 8). Modification of cAsp^{61} in the c-ring by *N*,*N*′-dicyclohexylcarbodiimide (DCCD) effectively inhibits ATPase activity of F_0F_1 embedded in nanodiscs (23), indicating that this ATPase-dependent rotation is linked to proton pumping across the lipid bilayer.

A major difference between a membrane and a nanodisc is that in the latter, which was used in the single-molecule experiments here, both half-channels are exposed to the same pH. The rate of F_1-ATPase activity measured in ensemble assays decreases with pH between pH 7.5 and 6.5 by ~2-fold (28), during which the increase in transient dwells is the greatest (Fig. 5). However, it is noteworthy that the rate-limiting step that determines ATPase activity occurs during the catalytic dwell, and not angular velocity of the power stroke (26), which can contribute to the formation of transient dwells (23). Thus, although the potential contribution of the pH dependence to the angular velocity of the F_1-ATPase cannot be ruled out, these data strongly suggest that the periplasmic half-channel is more easily protonated than is the cytoplasmic half-channel.

This preferential protonation of the periplasmic half-channel halts ATPase-driven rotation, and thereby blocks ATPase-

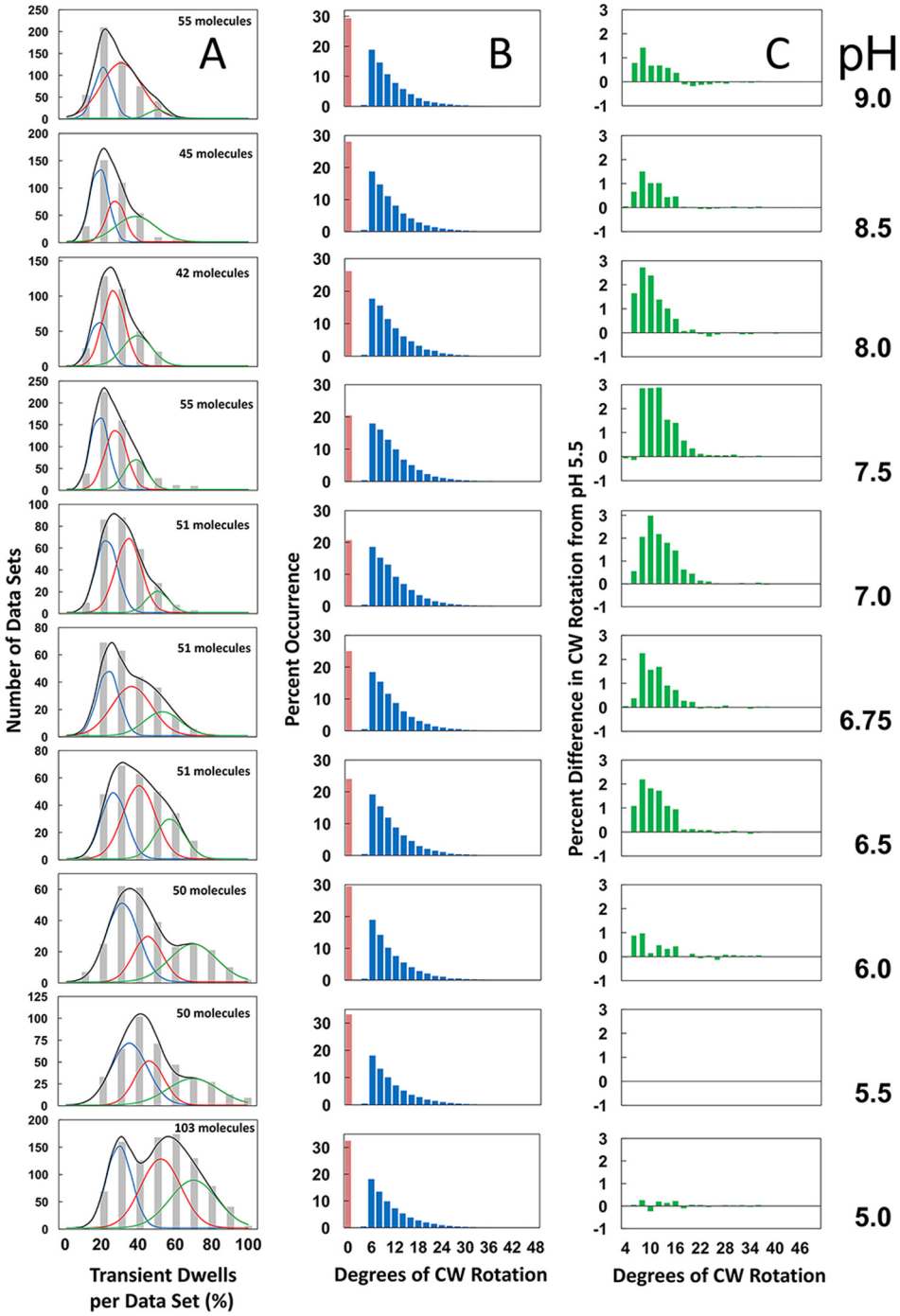

Figure 6. The pH dependence is shown. *A*, the distribution of single-molecule n-F_0F_1 power stroke data sets as a function of the percentage of the occurrence of transient dwells per data set, which were binned to each 10% (*gray bar graphs*). Each data set contained ~300 power strokes. The fit of the data to the sum of three Gaussians (*black line*) where the probability of forming transient dwells was low (*blue line*), medium (*red line*), and high (*green line*). The total number of n-F_0F_1 molecules examined at each pH is indicated. *B*, the distribution of the extent of F_0-dependent CW rotation against the force of F_1-ATPase–driven rotation. *C*, the difference in extent of CW rotation at each pH *versus* that observed at pH 5.5.

dependent proton pumping. Residues that contribute to proton translocation include aAsn^{214}, aGlu^{219}, aHis^{245}, and aGln^{252} in the periplasmic half-channel, and aGlu^{196} in the cytoplasmic half-channel (15–18). Several additional residues are likely to have a role, especially in the cytoplasmic half-channel that is currently less well defined.

When ATP synthase is driven by a high non-equilibrium pH gradient (ΔpH = 3), the periplasmic half-channel is exposed to a proton concentration 1000-fold higher than is the cytoplasmic channel. At such a high concentration, the groups in the former half-channel will be rapidly reprotonated after each donation of a proton to cAsp^{61}, which induces CW rotation of the c-ring, and minimizes the probability that the c-ring will subsequently rotate CCW. In response to CW rotation, a protonated cAsp^{61} moves into proximity of aGlu^{196} in the cytoplasmic half-channel. Presumably, the proton concentration is less than the p*K* of aGlu^{196}, and the sum of the other groups that participate in

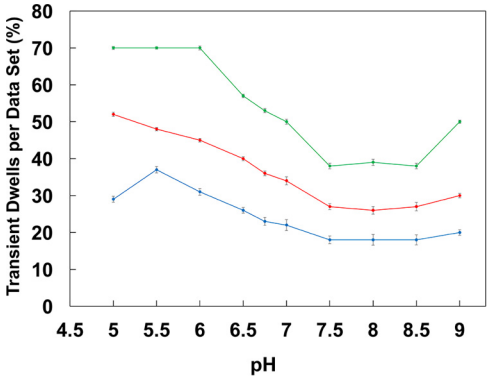

Figure 7. The pH dependencies of the average percent of transient dwells per data set derived from the Gaussian fits from Fig. 6 with low (*blue*), medium (*red*), and high (*green*) probabilities of transient dwell formation is shown. Vertical bars indicate standard error determined from the Gaussian curves of Fig. 6*A*.

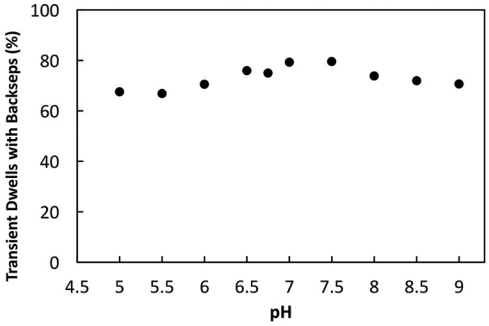

Figure 8. Average percentage of transient dwells in which the c-ring rotates CW against the force of F_1-ATPase–dependent CCW rotation as a function of pH is shown.

this half-channel such that dissociation of the proton into the cytoplasm is favored.

The concentration of protons required to protonate each half-channel is likely to depend on the number of groups that can be protonated, their aggregate accessibility to the adjacent aqueous phase, and their p*K*s, which depend on the hydrophobicity of their environments. The results presented here show that the ability to protonate the half-channels differs. Mutational studies are required to determine the relative contributions of subunit-a residues. These differences in the two half-channels have likely evolved to favor proton flux in the ATP synthase direction to minimize a futile cycle when the system has reached a steady state chemical gradient of ATP to ADP and P_i. In such a futile cycle, an ATP synthesized by proton flow would be immediately hydrolyzed to pump the protons in the opposite direction with no net gain in the storage of energy in the form of ATP. Without a bias that favors protonation of the ATP synthase half-channel, the magnitude of the chemical gradient that can be sustained will be diminished.

Single particle cryo-EM structures of F_0F_1 in the autoinhibited form (11) revealed three states (Fig. 9). The autoinhibited form of the ATP synthase from *E. coli* results when the C-terminal helix-turn-helix domain of the ϵ-subunit has become inserted into the core of the $(\alpha\beta)_3$-ring along the shaft of the γ-subunit in a manner that prevents rotation (29). The three structural states of this F_0F_1 structure are distinguished by the rotary positions of central stalk subunits γ and ϵ relative to the peripheral stalk that are separated by 120°, which is equivalent to the rotary positions of the drive shaft between ATPase-driven power strokes. It is noteworthy that single-molecule FRET measurements made where the donor and acceptor are attached to the central and peripheral stalks show a sequential low, medium, and high FRET signal when F_0F_1 embedded in proteoliposomes are actively synthesizing ATP in response to a proton gradient (3). The correlation between these FRET signals with the relative positions of the central and peripheral stalks in the three states of the *E. coli* cryo-EM structure suggests that the rotary positions of the γ and ϵ-subunits in these three states resemble that of the functional protein complex during each of the three F_1-ATPase catalytic dwells.

The data presented at each pH in Fig. 6*A* represent the sum of data sets typically from ~50 molecules of F_0F_1. The occurrence of transient dwells was analyzed for each molecule examined only from the power stroke in which the scattered light intensity of the nanorod progressed from a minimum through a maximum (Fig. 2), and not from the other two power strokes that complete a 360° rotation. For any given molecule, there is an equal probability that the power stroke analyzed corresponds to the rotation from one of the three structural states defined by the relative position of the two stalks. Thus, for every 51 F_0F_1 molecules analyzed for transient dwells, it is likely that the power strokes specific to each of the three different structural states will have been sampled by 17 molecules. This conclusion is supported by the observations that the distributions of transient dwell occurrence at any of the pH values examined do not fit to a single normal distribution, but that good fits to the data were achieved by fitting the distributions to the sum of three Gaussians (Fig. 6*A*).

The average values derived from each Gaussian dependence changed by a comparable extent as a function of pH (Fig. 7), which implies that the Gaussian curves represent molecules in which the probability of forming a transient dwell is low (*blue*), medium (*red*), or high (*green*). This suggests that the ATPase-driven power stroke that follows each of the three structural F_0F_1 states derived from cryo-EM has a low, medium, or high probability of forming transient dwells. In the absence of knowledge of the correlation between the ability to form transient dwells and the structural state of the power stroke examined, it is not possible at this time to know how the probability to form transient dwells in any one structural state changes with pH. It is noteworthy that because the ATPase rotates in 120° power strokes, the c-ring will rotate $4 \times 36°$ for one of the power strokes, but $3 \times 36°$ for the other two. Thus, it is possible that the probability of observing transient dwells is more likely for molecules aligned to step by four c-subunits per power stroke, although it does not explain the differences in the molecules with a low and medium probability of forming transient dwells.

The three states of *E. coli* F_0F_1 determined by cryo-EM (Fig. 9) differ not only by the relative position of the central and peripheral stalks, but also by the conformation of subunit-a, and its position on the c-ring. These differences include the positions of subunit-a residues $aAsn^{214}$, $aArg^{210}$, and $aGlu^{196}$ involved in proton translocation relative to the $cAsp^{61}$ residues on each c-subunit. In addition, the three structural states of *E. coli* F_0F_1 differ in the position of the subunit-a 3_{10}-helix II and

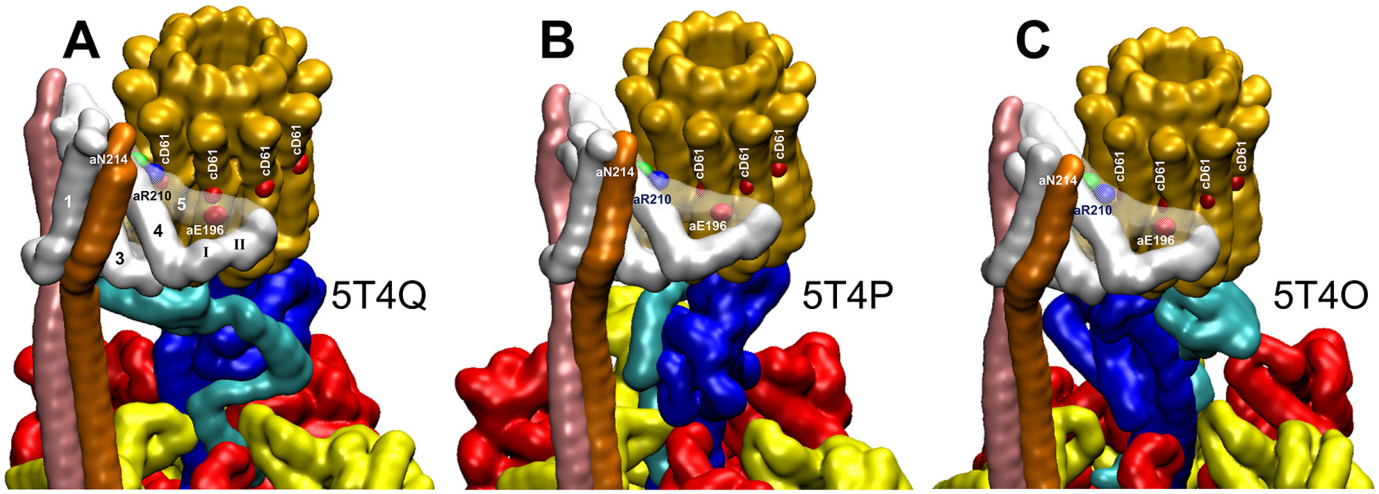

Figure 9. Conformational differences in the subunit-a relative to the c-ring between the three states of autoinhibited *E. coli* F_0F_1 as determined by cryo-EM is shown (11). *A–C*, states 1 (*A*), 2 (*B*), and 3 (*C*) are defined by the rotational positions of the central stalk relative to the peripheral stalk that result from the 120° power strokes (PDB reference IDs 5T4Q, 5T4P, and 5T4O, respectively). The autoinhibited state results from insertion of the C-terminal domain of subunit-ϵ into the core of the F_1 $(\alpha\beta)_3$-ring.

its subsequent loop relative to the c-ring. It is noteworthy that similar conformational changes were proposed in the grab and push mechanism to explain the basis of transient dwell formation, and the ability of subunit-a to push the c-ring CW against the force of ATPase-dependent rotation (18). The cryo-EM structures of *E. coli* F_0F_1 are in the autoinhibited state in which the C terminus of the ϵ-subunit has adopted a conformation that prevents rotation. Thus, it is not possible at this time to determine whether subunit-a has been trapped in different functional conformations that represent sequential steps in the grab and push mechanism or whether these conformational differences predispose a given rotational state of the complex to have a low, medium, or high probability of forming transient dwells.

Experimental procedures

Preparations of n-F_0F_1 ATPase

Detergent-solubilized F_0F_1 samples were expressed from the pNY_1-Ase plasmid construct that contained a Cys inserted at the second position of subunit-c (c2▽Cys) as described previously by Ishmukhametov *et al.* (23). The protein complex was purified, biotinylated, and incorporated into nanodiscs as described previously (23).

Single-molecule studies

Assembly of n-F_0F_1 complexes on a microscope slide and attachment of a 80 × 40-nm gold nanorod to the c-ring of each complex was carried out as described by Martin *et al.* (18). Rotation measurements were made in buffer containing 1 mM Mg^{2+} ATP, 10 mM KCl, 30 mM PIPES, and 30 mM Tris that was adjusted to the pH indicated. The assay to use changes in scattered light intensity from the nanorod to measure rotation of single molecules was as described by Hornung *et al.* (25). Briefly, light scattered from a single nanorod on the microscope slide (as shown in Fig. 2) was aligned with a pinhole, which then passed through a band-pass filter to eliminate all but red light, a polarizing filter, and a lens that focused the light on a single photon counter. Prior to data acquisition, the polarizing filter was rotated and light intensity changes were monitored at a frame rate equivalent to ~55 frames per second. At this slow frame rate, the observed changes in light intensity primarily represented the three rotational positions of the nanorod defined by the catalytic dwells of the F_1-ATPase that are separated by 120°. Attachment of the nanorod to an actively rotating n-F_0F_1 complex was confirmed by the change in the dynamic range of the changes in scattered light intensity as a function of the rotational position of the polarizing filter as described by Spetzler *et al.* (24). The filter was then rotated to align one of the catalytic dwells with a minimum of scattered light intensity. Rotation data were then acquired at 100 kHz in 5-s data sets. Power strokes that rotated the nanorod from a minimum through a maximum in scattered light intensity, which is equivalent to a 90° transition in position, were analyzed for the presence of transient dwells using custom software developed in MATLAB R2013b as described by Martin *et al.* (18).

Author contributions—W. F. conceived the project and obtained funding for it. S. Y. performed the experiments. S. Y. and W. F. designed the experiments, analyzed the data, and wrote the paper.

Acknowledgment—We thank Zain A. Bukhari for help in the preparation of Figure 6.

References

1. Spetzler, D., Ishmukhametov, R., Hornung, T., Martin, J., York, J., Jin-Day, L., and Frasch, W. D. (2012) Energy transduction by the two molecular motors of the F_1F_0 ATP synthase. In *Photosynthesis: Plastid Biology, Energy Conversion and Carbon Assimilation* (Eaton-Rye, J. J., Tripathy, B. C., and Sharkey, T. D., eds.), Advances in Photosynthesis and Respiration, Vol. 34, pp. 561–590, Springer, Dordrecht, The Netherlands
2. Stock, D., Leslie, A. G., and Walker, J. E. (1999) Molecular architecture of the rotary motor in ATP synthase. *Science* **286,** 1700–1705
3. Diez, M., Zimmermann, B., Börsch, M., König, M., Schweinberger, E., Steigmiller, S., Reuter, R., Felekyan, S., Kudryavtsev, V., Seidel, C. A., and Gräber, P. (2004) Proton-powered subunit rotation in single membrane-bound F_0F_1-ATP synthase. *Nat. Struct. Mol. Biol.* **11,** 135–141
4. Noji, H., Yasuda, R., Yoshida, M., and Kinosita, K., Jr. (1997) Direct observation of the rotation of F_1-ATPase. *Nature* **386,** 299–302

5. Spetzler, D., Ishmukhametov, R., Hornung, T., Day, L. J., Martin, J., and Frasch, W. D. (2009) Single molecule measurements of F_1-ATPase reveal an interdependence between the power stroke and the dwell duration. *Biochemistry* **48,** 7979–7985
6. Turina, P., Samoray, D., and Gräber, P. (2003) H^+/ATP ratio of proton transport-coupled ATP synthesis and hydrolysis catalysed by CF_0F_1-liposomes. *EMBO J.* **22,** 418–426
7. Kushmerick, M. J., Meyer, R. A., and Brown, T. R. (1992) Regulation of oxygen consumption in fast- and slow-twitch muscle. *Am. J. Physiol.* **263,** C598–C606
8. Kushmerick, M. J., Moerland, T. S., and Wiseman, R. W. (1992) Mammalian skeletal muscle fibers distinguished by contents of phosphocreatine, ATP, and P_i. *Proc. Natl. Acad. Sci. U.S.A.* **89,** 7521–7525
9. Abrahams, J. P., Leslie, A. G., Lutter, R., and Walker, J. E. (1994) Structure at 2.8 Å resolution of F_1-ATPase from bovine heart mitochondria. *Nature* **370,** 621–628
10. Adachi, K., Oiwa, K., Nishizaka, T., Furuike, S., Noji, H., Itoh, H., Yoshida, M., and Kinosita, K., Jr. (2007) Coupling of rotation and catalysis in F_1-ATPase revealed by single-molecule imaging and manipulation. *Cell* **130,** 309–321
11. Sobti, M., Smits, C., Wong, A. S., Ishmukhametov, R., Stock, D., Sandin, S., and Stewart, A. G. (2016) Cryo-EM structures of the autoinhibited *E. coli* ATP synthase in three rotational states. *eLife* **5,** e21598
12. Zhou, A., Rohou, A., Schep, D. G., Bason, J. V., Montgomery, M. G., Walker, J. E., Grigorieff, N., and Rubinstein, J. L. (2015) Structure and conformational states of the bovine mitochondrial ATP synthase by cryo-EM. *eLife* **4,** e10180
13. Allegretti, M., Klusch, N., Mills, D. J., Vonck, J., Kühlbrandt, W., and Davies, K. M. (2015) Horizontal membrane-intrinsic α-helices in the stator a-subunit of an F-type ATP synthase. *Nature* **521,** 237–240
14. Morales-Rios, E., Montgomery, M. G., Leslie, A. G. W., and Walker, J. E. (2015) Structure of ATP synthase from *Paracoccus denitrificans* determined by X-ray crystallography at 4.0 Å resolution. *Proc. Natl. Acad. Sci. U.S.A.* **112,** 13231–13236
15. Cain, B. D., and Simoni, R. D. (1988) Interaction between Glu-219 and His-245 within the a subunit of F_1F_0-ATPase in *Escherichia coli*. *J. Biol. Chem.* **263,** 6606–6612
16. Cain, B. D., and Simoni, R. D. (1989) Proton translocation by the F_1F_0 ATPase of *Escherichia coli.* Mutagenic analysis of the a subunit. *J. Biol. Chem.* **264,** 3292–3300
17. Vik, S. B., Cain, B. D., Chun, K. T., and Simoni, R. D. (1988) Mutagenesis of the α subunit of the F_1F_0-ATPase from *Escherichia coli.* Mutations at Glu-196, Pro-190, and Ser-199. *J. Biol. Chem.* **263,** 6599–6605
18. Martin, J., Hudson, J., Hornung, T., and Frasch, W. D. (2015) F_0-driven rotation in the ATP synthase direction against the force of F_1 ATPase in the F_0F_1 ATP synthase. *J. Biol. Chem.* **290,** 10717–10728
19. Lightowlers, R. N., Howitt, S. M., Hatch, L., Gibson, F., and Cox, G. B. (1987) The proton pore in the *Escherichia coli* F_0F_1-ATPase: A requirement for arginine at position 210 of the a-subunit. *Biochim. Biophys. Acta* **894,** 399–406
20. Etzold, C., Deckers-Hebestreit, G., and Altendorf, K. (1997) Turnover number of *Escherichia coli* F_0F_1 ATP synthase for ATP synthesis in membrane vesicles. *Eur. J. Biochem.* **243,** 336–343
21. Fischer, S., Etzold, C., Turina, P., Deckers-Hebestreit, G., Altendorf, K., and Gräber, P. (1994) ATP synthesis catalyzed by the ATP synthase of *Escherichia coli* reconstituted into liposomes. *Eur. J. Biochem.* **225,** 167–172
22. Engelbrecht, S., Deckers-Hebestreit, G., Altendorf, K., and Junge, W. (1989) Cross-reconstitution of the F_0F_1-ATP synthases of chloroplasts and *Escherichia coli* with special emphasis on subunit δ. *Eur. J. Biochem.* **181,** 485–491
23. Ishmukhametov, R., Hornung, T., Spetzler, D., and Frasch, W. D. (2010) Direct observation of stepped proteolipid ring rotation in *E. coli* F_0F_1 ATP synthase. *EMBO J.* **29,** 3911–3923
24. Spetzler, D., York, J., Daniel, D., Fromme, R., Lowry, D., and Frasch, W. (2006) Microsecond time scale rotation measurements of single F_1-ATPase molecules. *Biochemistry* **45,** 3117–3124
25. Hornung, T., Martin, J., Spetzler, D., Ishmukhametov, R., and Frasch, W. D. (2011) Microsecond resolution of single-molecule rotation catalyzed by molecular motors. *Methods Mol. Biol.* **778,** 273–289
26. Martin, J. L., Ishmukhametov, R., Hornung, T., Ahmad, Z., and Frasch, W. D. (2014) Anatomy of F_1-ATPase powered rotation. *Proc. Natl. Acad. Sci. U.S.A.* **111,** 3715–3720
27. Fillingame, R. H., and Steed, P. R. (2014) Half channels mediating H^+ transport and the mechanism of gating in the F_0 sector of *Escherichia coli* F_0F_1 ATP synthase. *Biochim. Biophys. Acta* **1837,** 1062–1068
28. Wilke-Mounts, S., Weber, J., Grell, E., and Senior, A. E. (1994) Tryptophan-free *Escherichia coli* F_1-ATPase. *Arch. Biochem. Biophys.* **309,** 363–368
29. Cingolani, G., and Duncan, T. M. (2011) Structure of the ATP synthase catalytic complex F_1 from *Escherichia coli* in an autoinhibited conformation. *Nat. Struct. Mol. Biol.* **18,** 701–707